J Mater Sci (2011) 46:4407–4412
DOI 10.1007/s10853-010-5017-z

IIB 2010

Mass transfer through a single grain boundary in alumina bicrystals under oxygen potential gradients

Tsuneaki Matsudaira · Satoshi Kitaoka · Naoya Shibata · Tsubasa Nakagawa · Yuichi Ikuhara

Received: 4 August 2010 / Accepted: 19 October 2010 / Published online: 2 November 2010

Abstract The mass-transfer behavior through grain boundaries (GBs) in alumina was systematically investigated using four types of alumina bicrystals. The alumina bicrystal wafers were exposed to the constant oxygen potential gradient (ΔP_{O_2}) generated by the combination of two different oxygen partial pressures $P_{O_2}(\mathrm{II})$ and $P_{O_2}(\mathrm{I})$ of 10^5 and 1 Pa, respectively, at 1923 K. Ridges were formed along the GBs on the surface subjected to $P_{O_2}(\mathrm{II})$, and deep GB ditches were developed on the $P_{O_2}(\mathrm{I})$ surface mainly during the migration of aluminum thorough GBs from the $P_{O_2}(\mathrm{I})$ surface to $P_{O_2}(\mathrm{II})$ surface. The surface morphology changes in the vicinity of the GBs were observed by atomic force microscopy. It was found that the surface morphology changes indicative of the aluminum GB diffusion were strongly dependent on the GB characteristics. The GB diffusion coefficients of aluminum estimated from the volume of the GB ridges showed a clear correlation to the local bonding environments of GB cores estimated from theoretical calculations reported previously.

T. Matsudaira (✉) · S. Kitaoka · Y. Ikuhara
Japan Fine Ceramics Center, 2-4-1 Mutsuno, Atsuta-ku, Nagoya 456-8587, Japan
e-mail: matsudaira@jfcc.or.jp

N. Shibata · Y. Ikuhara
Institute of Engineering Innovation, The University of Tokyo, Yayoi 2-11-16, Bunkyo-ku, Tokyo 113-8656, Japan

T. Nakagawa
National Institute for Materials Science, 1-2-1 Sengen, Tsukuba-shi, Ibaraki 305-0047, Japan

Introduction

Alumina-forming alloys are widely used for hot section components such as thermal barrier coating systems [1] under high operating temperatures and oxidizing environments. The excellent high-temperature performance of these alloys appears to be due to the formation of an alumina scale, which acts as a protective layer on the alloy against further oxidation. To save energy and reduce the use of alloys containing rare elements, it is highly desirable to further improve the high-temperature durability of such components. In this regard, suppressing mass transfer through the alumina scale is expected to markedly improve the durability of the alloys.

When oxidation of these alloys occurs through the alumina scale under high oxygen partial pressures (P_{O_2}), such as in air, the scale is exposed to steep oxygen potential gradient (ΔP_{O_2}) in the direction opposite to the aluminum potential gradient, in accordance with the Gibbs–Duhem equation. The scale grows on the alloys by an inward grain boundary (GB) diffusion of oxygen and an outward GB diffusion of aluminum, resulting in the development of GB ridges on the scale surfaces. In contrast, these ridges do not form in a low P_{O_2} environment, such as in a purified argon flow [2].

To clarify the mass-transfer mechanism for the above-mentioned phenomena, oxygen permeation through polycrystalline alumina wafers exposed to ΔP_{O_2} at high temperatures, with each surface of the wafer deliberately subjected to a different P_{O_2} values, was measured [3–9]. When a ΔP_{O_2} was generated by the combination of a $P_{O_2}(P_{O_2}(\mathrm{II}))$ value above 10^3 Pa and a constant $P_{O_2}(P_{O_2}(\mathrm{I}))$ value of 1 Pa at 1923 K, for example, oxygen permeated mainly via GB diffusion of aluminum through

aluminum vacancies from the $P_{O_2}(I)$ surface to the $P_{O_2}(II)$ surface, resulting in the formation of GB ridges on the $P_{O_2}(II)$ surface. As described in Refs. [3–6], O_2 molecules were adsorbed onto the surface at higher P_{O_2} and subsequently dissociated into oxygen ions (forming Al_2O_3), while oxygen ions on the opposite surface at lower P_{O_2} were desorbed by association into O_2 molecules (decomposition of Al_2O_3), resulting in apparent permeation of oxygen through the alumina wafers. The aluminum vacancies were likely induced as new defects in the neighborhood of the GBs by subjecting the wafer to ΔP_{O_2}. In other words, O_2 molecules were adsorbed onto the $P_{O_2}(II)$ surface and subsequently dissociated into oxygen ions according to Eq. 1 [3–6], resulting in the formation of alumina along the GB.

$$1/2O_2 \rightarrow O_O^X + 2/3V_{Al}''' + 2h^{\cdot} \quad (1)$$

The total volume of the GB ridges, measured by three-dimensional (3D) laser scanning microscopy, was consistent with the volume of alumina that should have been produced based on the detected amount of oxygen permeation [5]. This result supports the oxygen permeation mechanism presented in Eq. 1 under the ΔP_{O_2} produced by the higher P_{O_2} values. As reported in Refs. 3–6, when an oxygen potential gradient was generated by a combination of a $P_{O_2}(II)$ of 1 Pa and a $P_{O_2}(I)$ below 10^{-3} Pa at 1923 K through the polycrystalline alumina wafer, O_2 molecules are considered to permeate mainly by GB diffusion of oxygen through oxygen vacancies from the $P_{O_2}(II)$ surface to the $P_{O_2}(I)$ surface. In this case, very little ridge formation occurs at GBs because of the extremely low aluminum flux. The oxygen vacancies may be formed preferentially in the vicinity of the GBs due to the ΔP_{O_2}.

Many studies have focused on oxygen GB diffusion in polycrystalline alumina using either secondary ion mass spectroscopy (SIMS) [10–12] or nuclear reaction analysis (NRA) [13] to determine ^{18}O depth profiles after high-temperature exchange with ^{18}O-enriched oxygen. In contrast, there are few reports on aluminum diffusion coefficients, especially the GB diffusion coefficients of aluminum, because the appropriate tracer, ^{26}Al, has a very low specific activity and an extremely long half-life of 7.2×10^5 years [5, 6, 14, 15]. The GB diffusion coefficients of aluminum and oxygen in polycrystalline alumina have been recently reported on the basis of measurements of the P_{O_2} dependence on the oxygen permeability constants of alumina wafers exposed to ΔP_{O_2} at high temperatures, assuming that the flux of oxygen permeating through the wafer was due to a single species (aluminum or oxygen) under the particular ΔP_{O_2} conditions [5, 6]. The aluminum GB diffusion coefficients were found to increase with increasing P_{O_2}, in an inverse relationship to the P_{O_2} dependence on the oxygen GB diffusion coefficients. Because the GB ridges are not uniform on the polycrystalline alumina surfaces, the GB diffusion coefficients of aluminum may be strongly influenced by the GB characteristics and crystal orientation of the surface grains [5].

Evaluation of mass transfer through the GB in alumina bicrystals, in which the character of the GB can be arbitrarily controlled, is a very powerful method for understanding the fundamental mechanisms of GB phenomena such as creep and diffusion [11, 16–22]. For example, alumina bicrystals with [0001] axis tilt GBs were systematically fabricated, and their GB diffusivities of oxygen were experimentally measured [22]. The GB diffusivity of titanium was also evaluated as an indicator of aluminum GB diffusion [22]. In these cases, the GB diffusion coefficients of both oxygen and titanium were determined in homogeneous environments with no ΔP_{O_2}. It was found that the measured GB diffusion coefficients were strongly dependent on the atomic-scale GB structures. However, the effect of atomic-scale GB structures on the aluminum GB diffusion has not been clarified yet.

In this study, mass transfer through GBs in four types of alumina bicrystal wafers was evaluated under ΔP_{O_2} at high temperature, where aluminum mainly migrates through the GBs. The correlation between the aluminum GB diffusion coefficients and the GB structural characteristics will be discussed.

Experimental procedures

Fabrication of alumina bicrystals

The fabrication procedure of alumina bicrystals is in accordance with previous studies [11, 16, 18, 19, 21, 22]. Commercially available, high-purity sapphire single crystals (Shinkosha Co Ltd, Japan, purity >99.99 wt%) were used as a starting material. They were cut into dimensions of 7 × 15 × 15 mm, and their surfaces corresponding to the GB planes were mechanochemically polished using colloidal silica to obtain a mirror finish. The bicrystals were then joined at 1773 K for 10 h in air by a diffusion bonding technique. Figure 1 shows a schematic diagram of the crystallographic geometry of the alumina bicrystals fabricated in this study. The tilt angles 2θ between the $\vec{n}$ directions, Σ values, and the GB planes of the bicrystals are listed in Table 1. In this study, four different bicrystals were fabricated in terms of the GB coherency. The bicrystal denoted as Σ13 in Table 1 had a high coherent Σ13 $[1\bar{2}10]$ pyramidal twin GB, with a rotation axis of $[1\bar{2}10]$ [17–20]. On the other hand, the GBs denoted as Σ7a, Σ7m, and Σ31, with a common rotation axis of

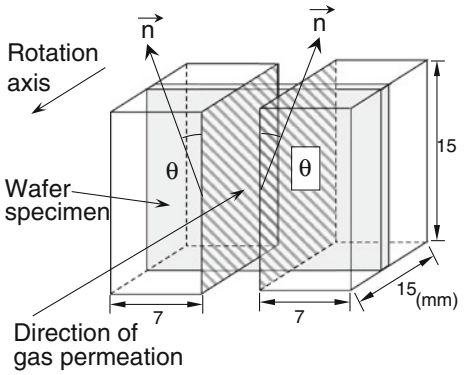

Fig. 1 Schematic diagram of the fabricated bicrystal Al_2O_3 wafers

Table 1 Tilt angles, Σ values, and grain boundary (GB) planes of the bicrystal Al_2O_3 wafers

Rotation axis	$\vec{n}$	2θ (deg.)	Σ	GB plane	Notation
$[1\bar{2}10]$	[0001]	103.6	13	$\{10\bar{1}4\}$	Σ13
[0001]	$[11\bar{2}0]$	38.2	7	$\{2\bar{3}10\}$	Σ7a
	$[1\bar{1}00]$	38.2	7	$\{4\bar{5}10\}$	Σ7m
		17.9	31	$\{7\bar{1}\bar{1}40\}$	Σ31

[0001], were less coherent than Σ13. The Σ31 bicrystal, which had the largest Σ value, had a Σ31 [0001] tilt GB, which was regarded as a general, random GB [11, 16, 22]. These bicrystals were cut into the wafers with dimensions of $\phi 11.5 \times 0.5$ mm, and exposed to ΔP_{O_2} at high temperatures. The wafer planes were set perpendicular to the rotation axis as shown in Fig. 1, and the surfaces were polished to a mirror finish.

Evaluation of the GB diffusivity of aluminum

The experimental conditions of the alumina bicrystal wafers exposed to ΔP_{O_2} at high temperature were the same as those in previous studies on polycrystalline alumina wafers [5, 6]. Each wafer was placed in between two alumina tubes in a furnace using Pt gaskets to create a seal between the wafer and the tubes by loading a weight on the top of the upper tube. The O_2 present as an impurity in the argon gas was monitored at the outlets of the upper and lower chambers enclosing the wafer and the alumina tubes, using a zirconia oxygen sensor at 973 K. A gas-tight seal was achieved in both chambers by heating at 1923 K. Subsequently, the measured P_{O_2} was regarded as a background level. Next, pure O_2 gas was introduced into the upper chamber at a flow rate of 1.67×10^{-6} m^3/s. Oxygen permeability constants for polycrystalline alumina wafers under this exposure condition were obtained on the order of 10^{-10} mol/m/s, and oxygen permeation occurred mainly by migration of aluminum thorough GBs from the lower $P_{O_2}(P_{O_2}(\mathrm{I}))$ surface to the higher $P_{O_2}(P_{O_2}(\mathrm{II}))$ surface. However, the oxygen permeability constants for the single crystal were below the lower detection limit ($<10^{-12}$ mol/m/s, 1923 K). Therefore, oxygen permeation preferentially occurred through the GBs [5]. For bicrystal wafers, oxygen permeation likely follows the same mass-transfer mechanism as in polycrystals. However, the GB lengths per unit surface area (GB density) in the bicrystal wafers were reduced by a factor of 10^5 compared with the polycrystalline alumina wafers. The oxygen permeability constant is proportional to the GB density, so even if the oxygen permeability constants for the bicrystals were similar to those of the polycrystals, the amount of permeated oxygen could not be precisely detected using the oxygen sensor, since it was below the lower detection limit. Oxygen permeation through the GB diffusion of aluminum from the $P_{O_2}(\mathrm{I})$ surface to $P_{O_2}(\mathrm{II})$ surface resulted in the formation of ridges at the GBs on the $P_{O_2}(\mathrm{II})$ surface. The total volume of the GB ridges on the polycrystalline wafer, measured by three-dimensional laser scanning microscopy, was consistent with the volume of alumina that should have been produced based on the observed amount of oxygen permeation [5]. Thus, the GB diffusion coefficient of aluminum determined from the GB ridge volume was almost the same as that determined by measuring the oxygen permeation.

In this study, therefore, the GB diffusion coefficients of aluminum were determined from the volume of the GB ridges on the $P_{O_2}(\mathrm{II})$ surfaces of the bicrystal wafers. The surface profiles around the GB on the bicrystal wafers exposed to $P_{O_2}(\mathrm{II})/P_{O_2}(\mathrm{I}) = 10^5/1$ Pa at 1923 K for 10 h were directly measured using an atomic force microscope (AFM, VM-8000, Keyence Co Ltd, Japan). The volume of a single GB ridge formed on the $P_{O_2}(\mathrm{II})$ surface was then estimated from its surface profile. The GB diffusion coefficients of aluminum were calculated on the assumption that the amount of permeated oxygen was equal to the oxygen content of the Al_2O_3 GB ridge volume in the following manner.

If the flux of the oxygen that permeates through the alumina wafer is controlled only by aluminum migration, according to Eq. 1, the flux of aluminum can be expressed in terms of the oxygen permeability constant, PL [5, 6],

$$\int_0^L J_{\mathrm{Al}} dx = A_{\mathrm{Al}}\left(P_{O_2}(\mathrm{II})^{3/16} - P_{O_2}(\mathrm{I})^{3/16}\right) = 4\mathrm{PL} \qquad (2)$$

where P is oxygen permeability, L is the wafer thickness, and A_{Al} is a constant. The second term in the parentheses of Eq. 2 can be ignored compared with the first term, because $P_{O_2}(\mathrm{II})$ and $P_{O_2}(\mathrm{I})$ were 10^5 and 1 Pa, respectively. If the GB ridge is assumed to be formed by aluminum GB migration, P can be rewritten as

$$P = \frac{3\rho_{Al_2O_3}}{2M_{Al_2O_3} \cdot t} \cdot V_{Al_2O_3} \quad (3)$$

where $V_{Al_2O_3}$ is the GB ridge volume per unit area, $\rho_{Al_2O_3}$ is the density of Al_2O_3, and $M_{Al_2O_3}$ is the molecular weight of Al_2O_3 and t is the exposure time. The P_{O_2} dependence of the aluminum GB diffusion coefficient, D_{Algb}, and P_{O_2} is given by

$$D_{Algb}\delta = \frac{A_{Al}}{12C_{Alb}S_{gb}} P_{O_2}(II)^{3/16} \quad (4)$$

where δ is the GB width, C_{Alb} is the molar concentration of aluminum per unit volume, and S_{gb} is the GB density [5, 6]. If the experimental value of A_{Al} is obtained using Eq. 2, $D_{Algb}\delta$ for a $P_{O_2}(II)$ can be calculated from Eq. 4.

Results and discussion

Surface morphology of bicrystal wafers

Figure 2 shows 3D AFM images of both surfaces of bicrystal wafers (Σ13, Σ7m, Σ7a, and Σ31) exposed at 1923 K for 10 h under ΔP_{O_2} with $P_{O_2}(II)/P_{O_2}(I) = 10^5/1$ Pa. Symmetrical surface profiles with respect to the GB planes were observed for all of the bicrystal wafers. Figure 3a and b shows magnified profiles of both surfaces of the Σ13 and Σ31 wafers, respectively. It was found that the morphology of surface profiles is strongly dependent upon the GB characteristics. For the wafers with relatively low GB coherence, such as Σ7a, Σ7m, and Σ31, as shown in Fig. 2, ridges were formed along the GBs on the $P_{O_2}(II)$ surfaces. Deep GB ditches were observed on the opposite $P_{O_2}(I)$ surfaces due to the migration of aluminum through GBs from the $P_{O_2}(I)$ surface to the $P_{O_2}(II)$ surface. The height of surface profiles around the GB decreased in the order of Σ31 > Σ7a > Σ7m. This suggests that the GB diffusivity of aluminum increases in the same order as the morphological change. For all bicrystals except for Σ3, peculiar two-stage ridges are found on the $P_{O_2}(II)$ surface, as shown in Figs. 2 and 3b. These unique ridges may be formed by the preferential vaporization at ridge tips with small curvature radii, followed by re-condensation at the ridge bases. Furthermore, for all the bicrystals except for Σ13, deep two-stage ditches were formed on the $P_{O_2}(I)$ surface. These ditches may be formed by the preferential decomposition of alumina at the bottom tip of the GB ditch during the GB diffusion of aluminum from the $P_{O_2}(I)$ surface to the $P_{O_2}(II)$ surface.

On the other hand, for the Σ13 bicrystal wafer, there was a shallow groove along the GB on both surfaces, as shown in Fig. 3a, similar to grooves formed by conventional

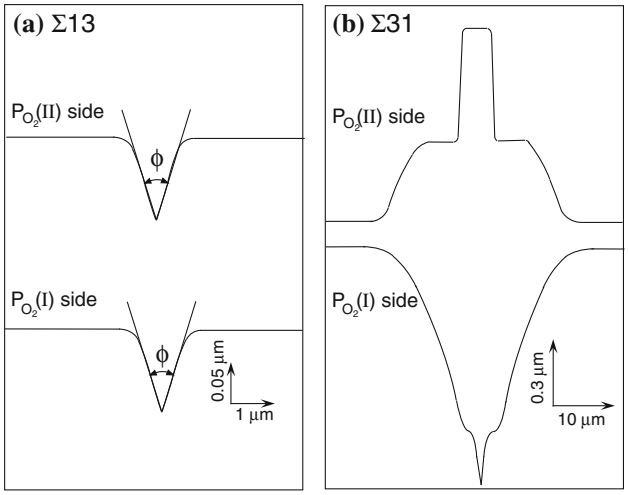

Fig. 3 AFM profiles of the surfaces of bicrystal Al_2O_3 wafers, **a** Σ13 and **b** Σ31, exposed at 1923 K for 10 h under ΔP_{O_2} with $P_{O_2}(II)/P_{O_2}(I) = 10^5/1$ Pa

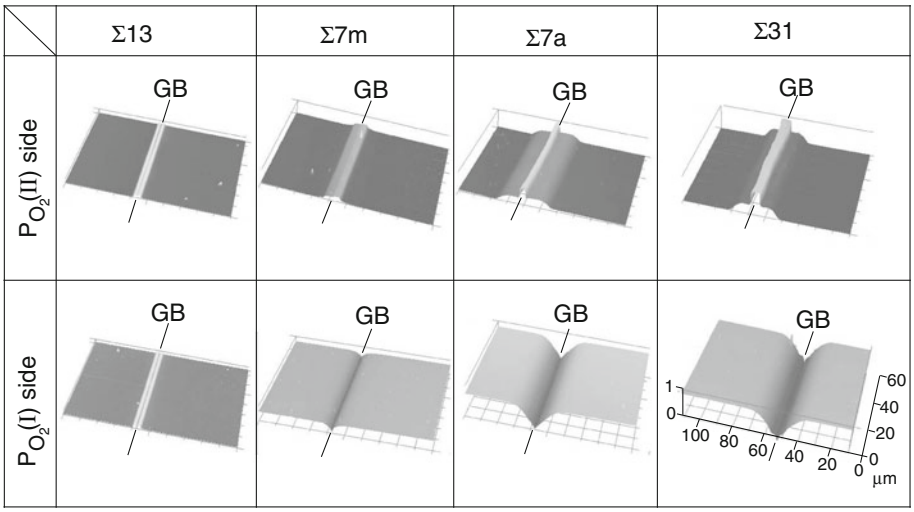

Fig. 2 AFM images of the surfaces of bicrystal Al_2O_3 wafers (Σ13, Σ7m, Σ7a, and Σ31) exposed at 1923 K for 10 h under ΔP_{O_2} with $P_{O_2}(II)/P_{O_2}(I) = 10^5/1$ Pa

thermal etching. There was neither a GB ridge on the $P_{O_2}(II)$ surface nor a ditch on the $P_{O_2}(I)$ surface, and no trace of the GB diffusion of aluminum. Therefore, migration of aluminum through the Σ13 wafer hardly occurs under the present experimental conditions. Since the surface profile of the Σ13 wafer was considered to have reached equilibrium, the GB energy (γ_{gb}) for Σ13 was determined from the groove angle ϕ in Fig. 3a and the surface energy (γ_S), as given by Eq. 5 [23]:

$$\gamma_{gb} = 2\gamma_S \cos\frac{\phi}{2} \quad (5)$$

γ_S for polycrystalline alumina is expressed as a function of temperature (T) in Eq. 6 [24]:

$$\gamma_S = 1839.9 - 0.474T \quad (6)$$

When γ_S for the $\{1\bar{2}10\}$ surface of the Σ13 wafer was assumed to be equal to that determined by Eq. 6 for the polycrystal (0.93 J/m^2), γ_{gb} for Σ13 at 1923 K is estimated to be 0.40 J/m^2 using Eqs. (5) and (6). γ_{gb} for the polycrystalline alumina at 1923 K was estimated to be 0.74 J/m^2 according to Ref. 23. The γ_{gb} calculated for Σ13 was smaller than the average of polycrystalline alumina because of its much higher GB coherency.

GB diffusion coefficients of aluminum

The GB diffusion coefficients of aluminum, $D_{gb}\delta$, were determined from the volume of the GB ridges observed on the $P_{O_2}(II)$ surfaces of the wafers. The volume includes a protuberance around the base of the ridge, because two-stage ridges were assumed to have resulted from aluminum GB diffusion. Table 2 summarizes $D_{gb}\delta$ of aluminum at 1923 K under $P_{O_2}(II)/P_{O_2}(I) = 10^5/1$ Pa, together with the value obtained from polycrystalline alumina under the same exposure conditions [5, 6]. $D_{gb}\delta$ ranged between 10^{-21} and 10^{-20} m^3/s, in the order of Σ31 > Σ7a > Σ7m. The $D_{gb}\delta$ for the Σ31 [0001] tilt GB (1.1×10^{-20} m^3/s) was found to be similar to that of the polycrystalline wafer (8.5×10^{-21} m^3/s).

An attempt to correlate GB atomic structure with GB mass-transfer behavior has been reported based on the stable atomic structures determined using static lattice calculations at 0 K without any ΔP_{O_2} [22]. For example, the mean bond length between aluminum and oxygen around the GB was estimated as the average of the fourth nearest-neighbor distances of Al–O bonds existing within 5 Å of the GB plane, and its correlation to GB mass-transfer behavior was considered [22]. Here, we also discuss the correlation between the aluminum GB diffusion coefficients listed in Table 2 and the mean Al–O bond lengths for each GB, although new defects may be preferentially introduced under ΔP_{O_2} in the present case. Figure 4 shows the $D_{gb}\delta$ values of the bicrystals under $P_{O_2}(II)/P_{O_2}(I) = 10^5/1$ Pa at 1923 K as functions of (a) calculated GB energy and (b) mean Al–O bond length as reported in Ref. 22. The $D_{gb}\delta$ values increase with both GB energy and mean Al–O bond length. The correlation factor between $D_{gb}\delta$ and the mean Al–O bond length (0.989) is closer to unity than that for the GB energy (0.931). Therefore, the $D_{gb}\delta$ values are thought to be more closely related to the mean Al–O bond length.

The increases in the Al–O mean bond length seem to be related to the decrease in oxygen coordination number of aluminum at the GB core region. According to the previous report [25], an increase in the oxygen coordination number was considered to decrease the GB diffusion coefficient of aluminum, based on the segregation of doped hafnium at GBs in polycrystalline alumina, where the oxygen coordination number of hafnium at the GBs was presumed to be larger than that of aluminum. Therefore, the increase in the

Table 2 $D_{gb}\delta$ of aluminum in bicrystal Al_2O_3 wafers (Σ13, Σ7m, Σ7a, and Σ31) at 1923 K under ΔP_{O_2} with $P_{O_2}(II)/P_{O_2}(I) = 10^5/1$ Pa

Specimen	$D_{gb}\delta$ of Al (m^3/s)
Bicrystal	
Σ7m	1.7×10^{-21}
Σ7a	7.4×10^{-21}
Σ31	1.1×10^{-20}
Polycrystalline [5, 6]	8.5×10^{-21}

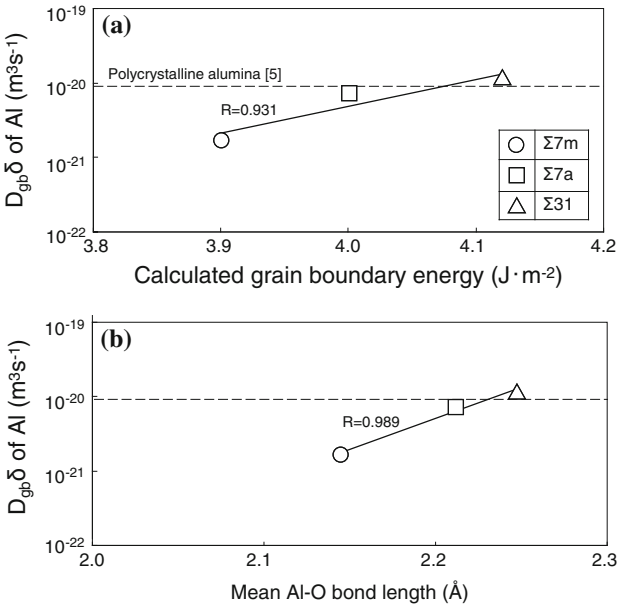

Fig. 4 The $D_{gb}\delta$ values of the bicrystals under $P_{O_2}(II)/P_{O_2}(I) = 10^5/1$ Pa at 1923 K as functions of **a** calculated GB energy and **b** mean Al–O bond length [22]

aluminum GB diffusion coefficients of the bicrystals may be related to a decrease in the oxygen coordination number of aluminum. For a Σ13 GB, since the mean Al–O bond length was estimated to be similar to that of an alpha-alumina perfect crystal (1.87–1.99 Å) [19], the aluminum $D_{gb}\delta$ for Σ13 is expected to be very low, in agreement with the present study.

Conclusions

Mass transfer through GBs in four types of alumina bicrystal wafers was evaluated under an oxygen potential gradient induced by a $P_{O_2}(II)/P_{O_2}(I)$ of 10^5 Pa/1 Pa at 1923 K. Decreasing the GB coherence of the bicrystals, the volume of the GB ridges formed on the $P_{O_2}(II)$ surface increased and the depth of the GB ditches observed on the $P_{O_2}(I)$ surface also increased, indicating an increase in the aluminum GB diffusion coefficients with decreasing GB coherence. The aluminum GB diffusion coefficient for a Σ31 [0001] tilt GB was almost the same as that obtained for a polycrystalline alumina wafer. The aluminum GB diffusion coefficients have a tendency to be proportional to the GB energies and the mean bond lengths between aluminum and oxygen around the GB. In contrast, no GB ridges or ditches are found on either surface of a highly coherent Σ13 $[1\bar{2}10]$ pyramidal twin GB. The aluminum GB diffusion coefficient in the Σ13 bicrystal is thus the lowest among the bicrystals examined in the present study.

Acknowledgement The authors are indebted to Mr. Y. Katsuyama, Keyence Co., Japan, for AFM surface profile measurements. This study was partially supported by the Grant-in-Aid for Scientific Research on Priority Areas "Nano Materials Science for Atomic Scale Modification 474" from the Ministry of Education, Culture, Sports, Science, and Technology (MEXT) of Japan.

References

1. Evans AG, Mumm DR, Hutchinson JW, Meier GH, Pettit FS (2001) Prog Mater Sci 46:505
2. Nychka JA, Clarke DR (2005) Oxid Metals 63:325
3. Matsudaira T, Wada M, Kitaoka S, Asai T, Miyachi Y, Kagiya Y (2008) J Soc Mater Sci Jpn 57:532
4. Wada M, Matsudaira T, Kitaoka S (2008) AMTC Lett 1:34
5. Kitaoka S, Matsudaira T, Wada M (2009) Mater Trans 50:1023
6. Matsudaira T, Wada M, Saitoh T, Kitaoka S (2010) Acta Mater 58:1544
7. Volk HF, Meszaros FW (1968) In: Fullhrath RM, Pask JA (eds) Ceramic micro structures their analysis significance and production. Wiley, New York, p 636
8. Courtright EL, Prater JT (1992) oxygen permeability of several oxides above 1200 °C, US DOE RepPNL-SA-20302:1
9. Ogura Y, Kondo M, Morimoto T, Notomi A, Sekigawa T (2001) Mater Trans 42:1124
10. Plot D, Gall ML, Lesage B, Huntz AM, Monty C (1996) Philos Mag A 73:935
11. Nakagawa T, Sakaguchi I, Shibata N, Matsunaga K, Mizoguchi T, Yamamoto T, Haneda H, Ikuhara Y (2007) Acta Mater 55:6627
12. Messaoudi K, Huntz AM, Lesage B (1998) Mater Sci Eng A 247:248
13. Heuer AH (2008) J Eur Ceram Soc 28:1495
14. Paladino AE, Kingery WD (1962) J Chem Phys 37:957
15. Le Gall M, Lesage B, Bernardini J (1994) Philos Mag A70:761
16. Buban JP, Matsunaga K, Chen J, Shibata N, Ching WY, Yamamoto T, Ikuhara Y (2006) Science 311:212
17. Fabris S, Elsasser C (2001) Phys Rev B 64:245117
18. Nakamura K, Shibata N, Matsunaga K, Yamamoto T, Ikuhara Y (2006) Trans Mater Res Soc Jpn 31:207
19. Nakamura K, Mizoguchi T, Shibata N, Matsunaga K, Yamamoto T, Ikuhara Y (2007) Phys Rev B 75:184109
20. Takahashi N, Mizoguchi T, Tohei T, Nakamura K, Nakagawa TT, Shibata N, Yamamoto T, Ikuhara Y (2009) Mater Trans 50:1019
21. Nishimura H, Matsunaga K, Saito T, Yamamoto T, Ikuhara Y (2003) J Am Ceram Soc 86:574
22. Nakagawa T (2008) Ph D thesis, Tokyo University, Japan, p 51
23. Nikolopoulos P (1985) J Mater Sci 20:3993. doi:10.1007/BF00552390
24. Levi G, Kaplan WD (2003) Acta Mater 51:2793
25. Kitaoka S, Matsudaira T, Wada M (2010) AMTC2 Lett 2:224